Electronic Supplementary Material (ESI) for Chemical Science.
This journal is © The Royal Society of Chemistry 2018

Supplementary Information

NIR-II Light-modulated Thermosensitive Hydrogel for Light-triggered Cisplatin Release and Repeatable Chemo-Photothermal Therapy

Changping Ruan[‡], *Chanjuan Liu* [‡], *Hailu Hu, Xiao-Lu Guo, Bang-Ping Jiang, Hong Liang and Xing-Can Shen**

State Key Laboratory for Chemistry and Molecular Engineering of Medicinal Resources
School of Chemistry and Pharmaceutical Science
Guangxi Normal University
Guilin, 541004, P. R. China
[‡]These authors contributed equally to this work.
Correspondence and requests for materials should be addressed to X.C.Shen
*E-mail: xcshen@mailbox.gxnu.edu.cn

Experimental Section

Reagents and Materials: N-phenylglycine (NPG), Ammonium persulfate (APS), and poly(ethylene glycol) (PEG, 6000) were obtained from Aladdin Regeants Co. Ltd. (Shanghai, China). H_2SO_4 (98%) and dimethylsulfoxide (DMSO) were obtained from Xilong Chemical Co. Ltd. (Guangdong, China). Penicillin-Streptomycin, *cis*-diamminedichloroplatinum (II) (CDDP), propidium iodide (PI), and 3-(4,5-dimethylthiazol-2-yl)-2,5-diphenyltetrazolium bromide (MTT) were bought from Sigma-Aldrich (USA). Calcein-AM was obtained from Invitrogen (USA). All chemicals were analytical grade and used as received without further purification unless otherwise noted. Deionized water was purified by a Millipore system.

Fetal bovine serum (FBS), trypsin, and RPMI-1640 medium were purchased from Gibco (New York, USA). The dialysis bags (8000–14 000Da) were obtained from Sinopharm Chemical Reagent Co. Ltd. (Shanghai, China). L929 cells, MDA-MB-231 and MCF-7 cells were supplied from Kunming Cell Bank of CAS (Kunming, China).

Synthesis: The PNPG-PEG composite was obtained via the polymerization of NPG in the presence of PEG. In a typical synthesis, 1.06 g of NPG was dissolved into 50 ml of 0.1 M H_2SO_4 aqueous solution. The mixture was stirred with magnetic stirring in ice water bath for 10 minutes. Then, 15 g of PEG was added into the mixture, followed by magnetic stirring of 30 minutes. The obtained solution containing NPG, PEG and H_2SO_4 was denoted as solution A. Simultaneously, 1.60 g of ammonium persulfate (APS) was dissolved into 50 ml of 0.1 M H_2SO_4 aqueous solution to form solution B. The solution B was dropwise added into solution A within in 3 hours under magnetic stirring in an ice water bath. The ice water bath was maintained for 5 hours. After 24 hours of stirring, a dark green solution was obtained. The as-prepared solution was purified by dialysis (8000–14 000Da) in de-ionized (DI) water for three days (water was renewed 3 times each day). The freeze-dried PNPG-PEG powder was obtained by lyophilization.

A typical PNPG-PEG/*a*-CD hydrogel was prepared by mixing equal volumes of PNPG-PEG (30 mg mL^{-1}) and *a*-CD (140 mg mL^{-1}) aqueous solution and then leaving the mixture to remain undisturbed for several minutes. To prepare the CDDP-laden hydrogel (CDDP /PNPG-PEG/*a*-CD hydrogel), the CDDP was previously dissolved into the PNPG-PEG dispersed aqueous suspension and then the same gelation procedure was performed. The sol-gel transition temperature of hydrogel was determined by test-tube inverting method.

Characterization: The FT-IR spectra were performed on a Perkin Elmer FT-IR spectrometer. The UV–vis–NIR spectra were collected from 300–1400 nm by Lambda 45 UV–vis–NIR spectrophotometer (Perkin Elmer, USA). The thermogravimetric analysis (TGA) was carried out on LABSYS evo thermogravimetric analyzer under nitrogen atmosphere from ambient temperature to 900 ℃, with a ramp rate of 10 ℃ min^{-1}. The photothermal images were taken by Infrared camera (MAG30, Magnity Electronics, China). The XRD patterns were recorded on a D8 ADVANCE (Germany) using Cu-Kα (0.15406 nm) radiation. The ICP measurements were conducted using the Thermo/Jarrell Ash Advantage Atomscan Inductively Coupled Argon Plasma Spectrometer. The scanning electron microscopy (SEM) images were collected on an FEI/Philips XL30ESEM-FEG field emission scanning electron microscopy system. The transmission electron microscopy (TEM) images were carried out on JEM100C ×II (JEOL, Japan). Rheological test was performed on a Malvern Kinexus lab+ rotational rheometer using 40 mm parallel-plate geometry, the gap distance between the two plates was fixed at 0.8 mm.

Calculation of the photothermal conversion efficiency: The photothermal conversion efficiency (η) of PNPG-PEG composite was calculated according to the following equations, as reported by literature [1, 2]:

$$\eta = \frac{hA\Delta T_{max} - Q_S}{I(1-10^{-A_\lambda})} \quad (1)$$

Where h was heat-transfer coefficient, A was the surface area of the container, I was the laser power, A_λ was the absorbance of the photothermal conversion agent (PNPG-PEG composite, at 808 nm and 1064 nm respectively), Q_s was the heat associated with the light absorbance of the solvent (water), which was measured independently using pure water without PNPG-PEG. ΔT_{max} was the temperature change at the maximum steady-state temperature ($\Delta T_{max} = T_{max} - T_{surr}$, T_{max} was the equilibrium temperature, representing no heat conduction away from the system surface by air; T_{surr} was ambient temperature of the surroundings). Thus, only the hA were unknown for the calculation of η.

In order to get the hA, we herein introduce θ, which is defined as the ratio of ΔT to ΔT_{max}.

$$\theta = \frac{\Delta T}{\Delta T_{\max}} \tag{2}$$

ΔT was the temperature change, which is defined as $T - T_{surr}$, (T and T_{surr} were the solution temperature and ambient temperature of the surroundings, respectively).

$$hA = \frac{mC_{\mathrm{p}}}{\tau} \tag{3}$$

At the cooling period of PNPG-PEG composite dispersion, $t = -\tau \ln\theta$, t was the time of cooling period. C_p and m were the heat capacity and the mass of solvent (water), τ was the time constant of heat transfer and determined by applying the linear time data from the cooling period *vs* $-\ln\theta$ (τ was the slope of bule line in **Figure S13b** and **S14b**). Substituting hA value into equation 1, the photothermal conversion efficiency (η) of PNPG-PEG can be calculated.

In vitro CDDP release: To prepare the CDDP-laden hydrogel (denoted as CDDP/PNPG-PEG/*a*-CD hydrogel, CDDP concentration: 0.5 mg mL^{-1}), the CDDP was previously dissolved into the PNPG-PEG dispersed aqueous suspension and then the same gelation

procedure as that of the PNPG-PEG/*a*-CD hydrogel was performed. Briefly, the CDDP was previously dissolved into the PNPG-PEG dispersed aqueous suspension (concentration of CDDP: 1.0 mg mL^{-1}) to form the solution A. Then, the obtained solution A (0.5 mL; PNPG-PEG: 30 mg mL^{-1}; CDDP: 1.0 mg mL^{-1}) was mixed with equal volumes of *a*-CD (0.5 mL; 140 mg mL^{-1}) to form a homogeneous precursor solution. The precursor solution was left undisturbed for several minutes to form the CDDP/PNPG-PEG/*a*-CD hydrogel. The obtained CDDP/PNPG-PEG/*a*-CD hydrogel (1.0 mL; concentration of CDDP: 0.5 mg mL^{-1}) were transferred into 10 mL vials. Then, 5 mL of PBS solution was added into the system. The vials were shaken at a rate of 50 strokes per minute. At pre-determined intervals, 5 mL of released medium were taken out, and an equal volume of fresh solution was added to keep a constant volume. The on-demand release of CDDP was performed under 1064 nm NIR laser irradiation for 5 minutes each time (0.5 W cm^{-2}). 4 cycles of laser on (5 minutes) and off (5 minutes) processes were performed. The concentration of CDDP in the release medium was determined by using ICP-MS.

Photothermal Imaging: The photothermal images of *a*-CD aqueous solution (70 mg mL^{-1}), PNPG-PEG aqueous solution (15 mg mL^{-1}), PNPG-PEG/*a*-CD hydrogel, and CDDP/PNPG-PEG/*a*-CD hydrogel (concentration of CDDP: 0.5 mg mL^{-1}) were taken by an infrared camera (MAG30, Magnity Electronics, China) under the irradiation of the 808 nm and 1064 nm laser (laser power: 0.5 W cm^{-2}; irradiation time: 5 minutes, unless noted otherwise), respectively. The temperature evolutions at different time intervals were analyzed with Magnity Electronics tools systems.

Biocompatibility evaluation: The biocompatibility of PNPG-PEG/*a*-CD hydrogels was evaluated by MTT assay and Live/Dead staining assay. To differentiate live (green) and dead (red) cells, the cells were co-stained by Calcine AM and propidium iodide (PI) and visualized

using fluorescence microscopy. MTT assay was used to quantitatively evaluate the cell viability at various hydrogel concentrations.

Cell Culture: The cells (L929 cells, MCF-7 cells, and MDA-MB-231 cells) were cultured in RPMI-DMEM medium containing with 1% penicillin streptomycin and 10% fetal bovine serum (FBS) and incubated in a humidified incubator containing 5% CO_2 at 37°C.

MTT assay: The cells (L929 cells, MCF-7 cells, and MDA-MB-231 cells, with a density of 1×10^4 cells per milliliter) were seeded in a 96-well plate at a density of 180 μL per well at 37 ℃ under 5% CO_2 for 24 h. Then, the PNPG-PEG/*a*-CD hydrogel was added to each well with different amount (concentration of hydrogel: 2, 4, 6, 8 and 10 mg mL^{-1}; n = 5 for each group). For the control group, same amount of phosphate buffered saline (PBS) solution was added. The plates were incubated in a humidified incubator containing 5% CO_2 at 37°C. After 48 hours of incubation, cell culture medium was removed and cells were rinsed with 200 μL of PBS solution for three times. Thereafter, 180 μL of fresh culture medium was added into the cells. Subsequently, 10 μL of MTT solution (with a concentration of 5 mg mL^{-1}) was added into each well. After 4 hours of incubation at 37°C, the cell cytotoxicity was assessed by MTT assay, measured at 570 nm using an Infinite M1000 UV-Vis microplate reader (TECAN, Austria). The groups treated with PBS solution were used as controls.

Live/Dead staining assay: The biocompatibility of the PNPG-PEG/*a*-CD hydrogels was also evaluated by staining L929 cells with Calcein-AM (1.6%, for live cells, green fluorescence) and propidium iodide (PI, 2 %, for dead cells, red fluorescence). Briefly, 400 μL of L929 cells (with a density of 1×10^5 cells per milliliter) in a clean 48-well plate were incubated for 24 hours in a humidified incubator containing 5% CO_2 at 37°C. Then, PNPG-PEG/*a*-CD hydrogel was added into the cell suspension and maintained at 37°C in a humidified incubator for 48 hours (concentration of hydrogel: 8 mg mL^{-1}). Cell culture medium was removed and cells were rinsed with PBS for three times. Thereafter, 400 μL of

fresh culture medium was added into the cells. Subsequently, Calcium-AM/PI was added into the 48-well plates to stain the cells, and these cells were incubated for another 20 minutes. Then, the stained cells were visualized using fluorescence microscopy on an inverted microscope (Olympus-IX51, Japan).

***In vitro* photothermal performance of PNPG-PEG/*a*-CD hydrogel:** The MDA-MB-231 cells were cultured in RPMI-DMEM medium containing with 1% penicillin streptomycin and 10% fetal bovine serum (FBS) and incubated for 24 hours in a humidified incubator containing 5% CO_2 at 37°C. Then, the cells were seeded into 24-well plates at a density of 1×10^5 cells per milliliter (800 μL per well) and incubated at 37 ℃ under 5% CO_2. The as-prepared PNPG-PEG/*a*-CD hydrogel was added into the cells and maintained at 37°C in a humidified incubator for 4 hours (with a concentration of 8 mg mL^{-1}) and followed by 1064 nm laser irradiation for different period of time (0, 1, 3, 5 minutes; at 0.5 W cm^{-2}). After 4 hours of incubation, the cell viability was evaluated by Live/Dead staining assay.

***In vitro* cell-killing efficacy of different administrations:** The *in vitro* cell-killing efficacy of different administrations (5 groups: treated with saline, free CDDP, PNPG-PEG/*a*-CD with 1064 nm laser irradiation, CDDP/PNPG-PEG/*a*-CD without laser irradiation, and CDDP/PNPG-PEG/*a*-CD with 1064 nm laser irradiation) were evaluated by assessing the viabilities of MDA-MB-231 cells using MTT assay. The MDA-MB-231 cells were seeded into 96-well plates at a density of 1×10^4 cells per milliliter (180 μL per well) and incubated at 37 ℃ under 5% CO_2. Subsequently, different formulations were added into the cell suspension and maintained at 37°C in a humidified incubator for 48 hours. The concentration of hydrogel and CDDP was 8 mg mL^{-1} and 40 μmol L^{-1}, respectively. For the laser treated groups, the laser irradiation was performed for 5 minutes at 0.5 W cm^{-2} after the 48 hours of incubation. Thereafter, the cell viability and proliferation were investigated using MTT assay.

***In vivo* gel formation:** To examine the injectability and *in vivo* gelation of the system, 200 μL precursor solutions of PNPG-PEG/*α*-CD (the mixture of 100 μL PNPG-PEG (30 mg mL^{-1}) and 100 μL *a*-CD (140 mg mL^{-1})) were subcutaneously injected into the Kunming mice. To minimize the loss of the material related to diffusion, the precursor solutions were injected about 8 to 10 minutes after the mixing. To observe the gel morphology, the mice were sacrificed after 30 minutes, 3 days, 7 days, 14 days, and 28 days of the injection, respectively. Haematoxylin and eosin (H&E) staining of the subcutaneous tissues surrounding the hydrogel was performed to estimate the biocompatibility of the hydrogel in *vivo*. The tissues were fixed with 10% formalin and embedded in paraffin for histological analysis using haematoxylin-eosin (H&E) stains.

***In vivo* antitumor activity:** Female BALB/c nude mice (5-6 weeks, 22 ±2g) bearing with MDA-MB-231 solid tumors were employed as animal model to investigate *in vivo* antitumor effects of different administrations. The tumor-bearing mice were supplied by Li Ke Aida Biotechnology Co. Ltd. (Beijing, China). To prepare the tumor-bearing mice, MDA-MB-231 tumor tissues (volume: 2×3×3 mm^3) was implanted into the right hind hip of each mouse. When the tumor volume reached to approximately 60-100 mm^3 (about one week after the inoculation of tumors tissues), the mice were randomly divided into eight groups (three mice for each group) to accept different treatments. Animals bearing implanted tumors were treated with intratumoral injection of: (1, 2) 100 μL of saline; (3, 4) 100 μL of free CDDP solution by multiple injections (at total doses of 8 mg CDDP/kg body weight; injection of 2 mg CDDP/kg body weight at day 0, 2, 4, 6, respectively); (5, 6) 100 μL of PNPG-PEG/*a*-CD hydrogel ((*via* a single injection); and (7, 8) 100 μL of CDDP/PNPG-PEG/*a*-CD hydrogel (*via* a single injection, at doses of 8 mg CDDP/kg body weight), respectively. For the groups injected with hydrogel (group 5, 6, 7, 8), the injected solution was prepared by mixing equal volumes of PNPG-PEG (50 μL, 30 mg mL^{-1}) and *a*-CD (50 μL, 140 mg mL^{-1}) aqueous solution. The

mixture was in solution state within several minutes before the injection and was injected about 8-10 minutes after the mixing of the solution. For the groups treated with CDDP/PNPG-PEG/*a*-CD hydrogel (group 7, 8), the CDDP was previously dissolved into the PNPG-PEG dispersed aqueous suspension to form a homogeneous solution. 4 hours after the injections, the groups labeled with 2, 4, 6, and 8 were treated with the first cycle of 1064 nm laser irradiation (5 minutes; power density: 0.5 W cm^{-2}) at the tumor sites. During the period of administrations, groups 2, 4, 6, and 8 were treated with a total of four cycles of 1064 nm laser irradiation (at 0, 2, 4 and 6 days following injections, 5 minutes each cycle; under a low power density of 0.5 W cm^{-2}). The corresponding temperature change and spatial temperature distribution in tumors of the groups exposed to laser irradiation was monitored by an Infrared thermal camera (MAG30, Magnity Electronics, China). Tumor sizes and body weight of each animal were monitored every day over a period of 2 weeks. Tumor volumes (V) were calculated according to the length (L) and width (W) of tumor ($V = L \times W^2/2$). The relative change rate (%) of body weight was estimated based on the following equation: relative change rate (%) = $[(W_i - W_0)/W_0] \times 100\%$; Here, W_0 and W_i was the weight of the mice before and during the treatment, respectively.

At the end of the administrations, mice were sacrificed, and the tumors and major organs (including heart, liver, spleen, lung and kidney) were excised, weighed and sectioned for pathological analysis. The tissues were fixed with 10% formalin and embedded in paraffin for histological analysis using haematoxylin-eosin (H&E) stains. All animal experimental procedures were carried out in compliance with the policies of the *Animal Care and Use Committee* of *Guangxi Medical University* (Nanning, China) and were approved by the local *Animal Care and Use Committee.*

Statistical Analysis

Statistical differences were analyzed using the one-way analysis of variance (ANOVA).

Statistical significance was set to *P < 0.05. All data were expressed as mean ± standard deviation (SD).

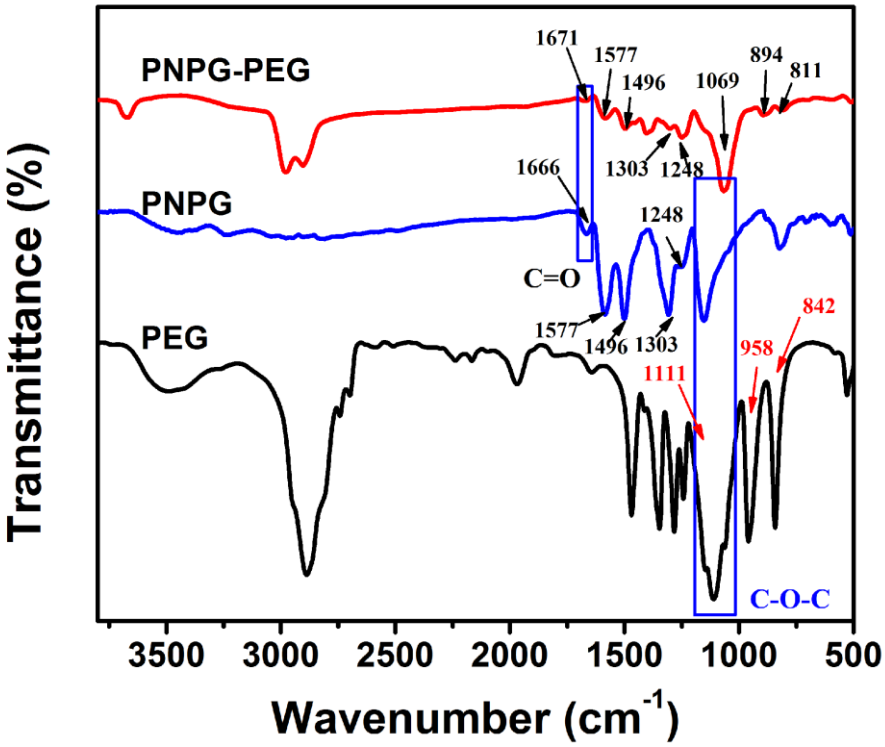

Figure S1. FT-IR spectra of PNPG-PEG compared with PEG and PNPG. For PNPG-PEG, the bands at 1577 and 1496 cm^{-1} were related to stretching vibrations of the quinonoid and benzenoid structure of PNPG, similar as that of PNPG polymer without the presence of PEG. [3] The peaks located at 1303 cm^{-1} and 1248 cm^{-1} was corresponded to the C-N stretching vibration.[3-6] The stretching vibration absorption of C=O in PNPG shifted from 1666 cm^{-1} to 1671 cm^{-1} in PNPG-PEG. The C–O–C stretching vibration, C–O–C deformation vibration, and C–O stretching vibration for PEG were located at 1111 cm^{-1}, 958 cm^{-1} and 842 cm^{-1}, respectively. Whereas these bands shifted to 1069 cm^{-1}, 894 cm^{-1}, and 811 cm^{-1} in PNPG-PEG, these observations indicated the hydrogen bonding interaction between PEG and PNPG in the PNPG-PEG composite.[4-6]

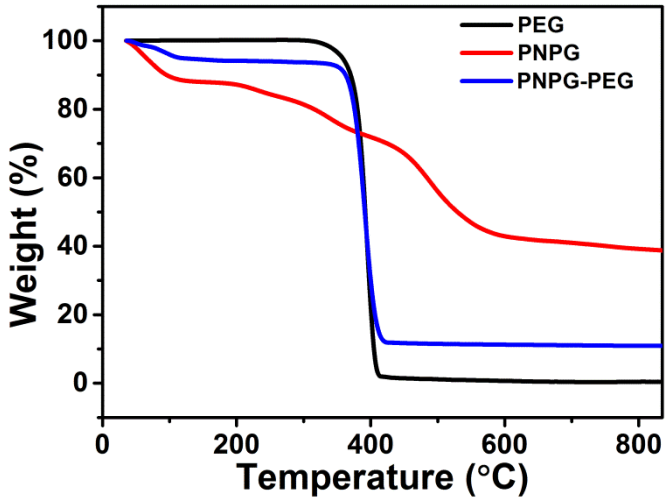

Figure S2. TGA of PEG, PNPG and PNPG-PEG composite. It was estimated that the PNPG-PEG composite was composed of 75% PEG and 25% PNPG (by weight).

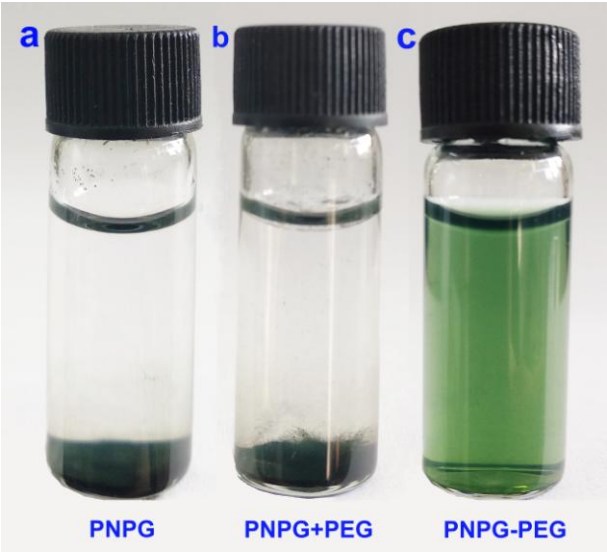

Figure S3. Digital photographs of (a) PNPG, (b) PNPG+PEG, and PNPG-PEG composite in water. The PNPG-PEG composite was highly water-soluble owing to the interaction between PNPG and PEG (c). In contrast, the PNPG polymer showed poor dispersibility and formed precipitation both in water (a) and in PEG solution (b). This observation provided indirect evidence of the hydrogen bonding interaction between PEG and PNPG in the PNPG-PEG composite.

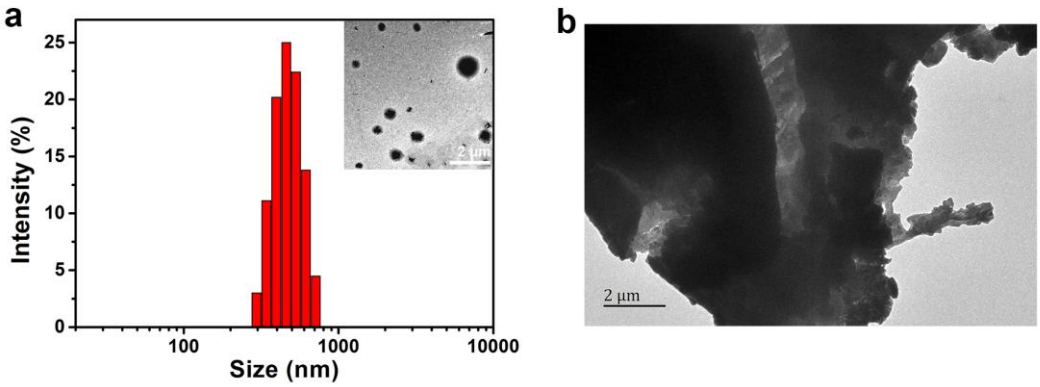

Figure S4. (a) Size distribution and TEM image of PNPG-PEG composite; (b) TEM image of PNPG.

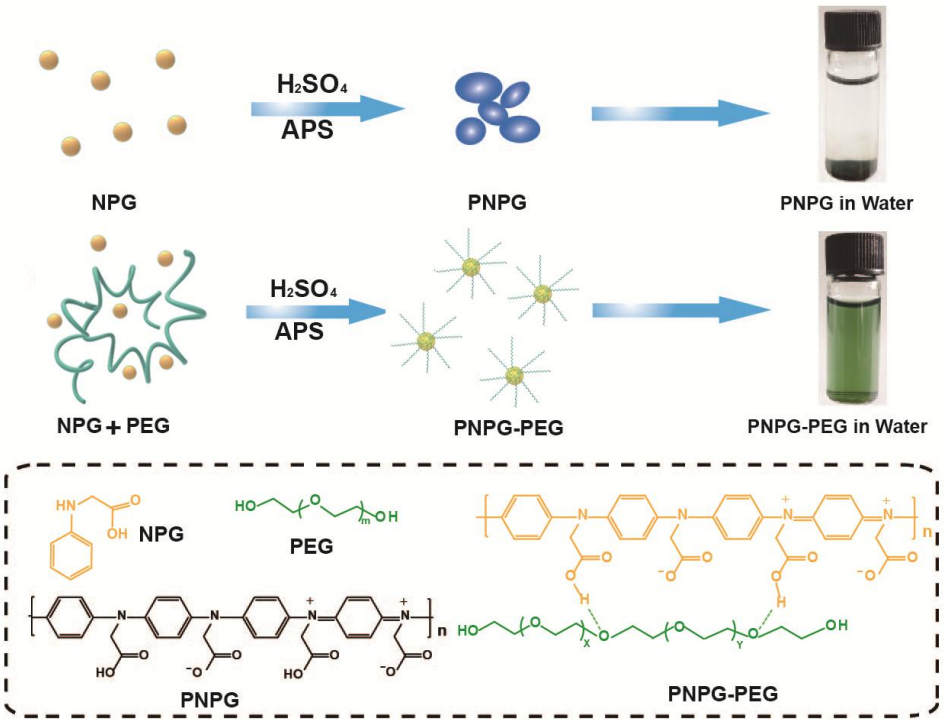

Figure S5. Schematic illustration of the formation of PNPG and PNPG-PEG composite. In the absence of PEG, the N-phenylglycine (NPG) formed hydrophobic polymer chains through the polymerization of monomer molecules. Consequently, the obtained PNPG polymer showed poor dispersibility and formed precipitation in water. It is likely that the PEG chains could prevent the uncontrolled polymerization of NPG monomer and the formation of large particles size. In the presence of PEG chains, the –COOH groups of NPG interacted with the oxygen atoms in PEG *via* hydrogen bonding interaction. Upon the polymerization of NPG monomers, the obtained PNPG polymer chains interacted with PEG chains through hydrogen-bond interactions and physical entanglements, thus allowing the formation of the water-soluble PNPG-PEG composite.

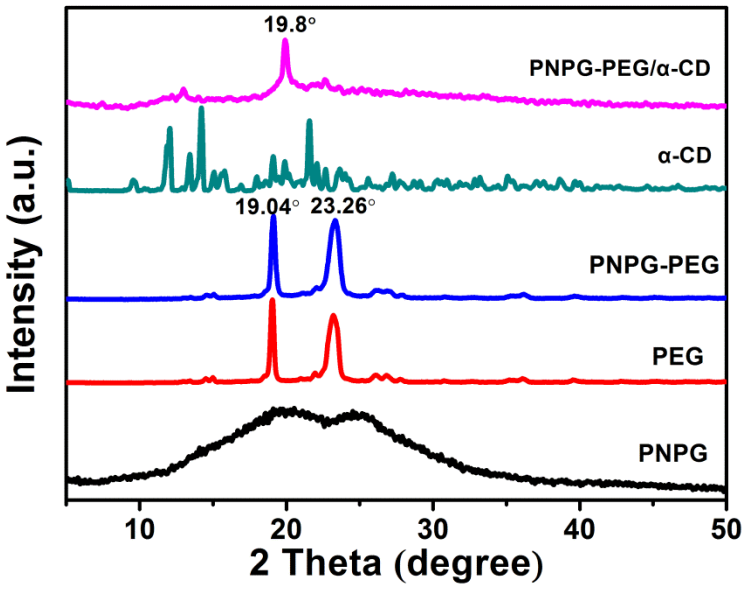

Figure S6. XRD diffraction patterns of PNPG-PEG/*α*-CD hydrogel compared with controls. The peak located at 19.8 ° was attributed to the column crystalline complex of PEG/*α*-CD inclusion, confirming the formation of PPRs.[7, 8]

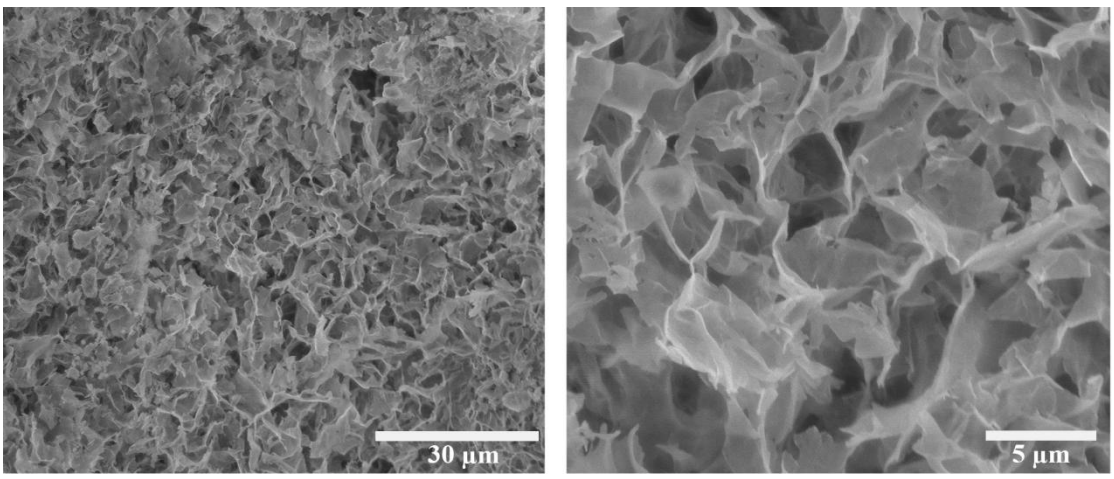

Figure S7. SEM images of PNPG-PEG/*α*-CD hydrogel showing the porous structure of the dried gel network.

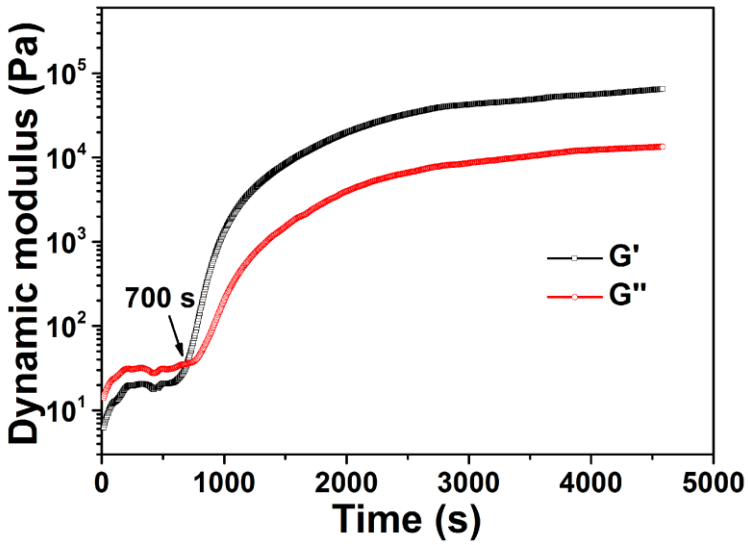

Figure S8. The elastic modulus (G') and viscous modulus (G") as a function of time for the as-prepared PNPG-PEG/*a*-CD hydrogel (gap: 0.8 mm, strain: 1 %, frequency: 1 Hz). The sample was prepared by mixing equal volumes of PNPG-PEG (0.5 mL, 30 mg mL^{-1}) and *a*-CD (0.5 mL, 140 mg mL^{-1}) aqueous solution, and then was put into 40 mm parallel-plate geometry for rheological analysis.G' is the shear storage or elastic modulus, and G" is the shear loss or viscous modulus. G' provides information about the elasticity or the stored deformation energy, whereas G" represents the viscous character or the amount of energy dissipated as heat.[9] Both G' and G" increased along with the time and reached a plateau finally. The increase of G' and G" values of the hydrogel along with the time implied that the crosslinking density of the hydrogels was increased owing to the increased numbers of host-guest inclusions and the physical cross-links. The crosslink of the storage (G') and loss (G") moduli indicated the occurrence of sol-gel translation (in about 12 minutes).[10,11]

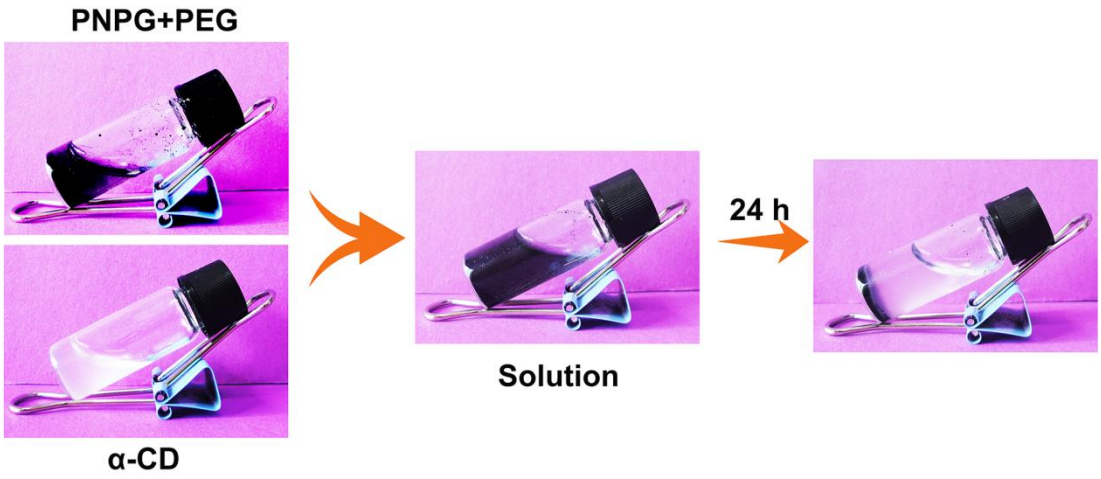

Figure S9. Digital photographs illustrating that the direct mixing of PNPG and PEG with *α*-CD did not generate a hydrogel. The failure of gelation was probably ascribed to the uncontrolled host-guest inclusion between free PEG chains and *α*-CD. This provided indirect evidence that PNPG polymer served as a core material to tether PEG chains in PNPG-PEG/*α*-CD hydrogel, which was indispensable for the formation of the supramolecular hydrogel More specifically, the tethering of the PEG chains by PNPG was able to prevent the complete inclusion of *α*-CD on the PEG chain and additionally provide stable and constant physical cross-links, both of which were beneficial for the hydrogel formation [8, 11]

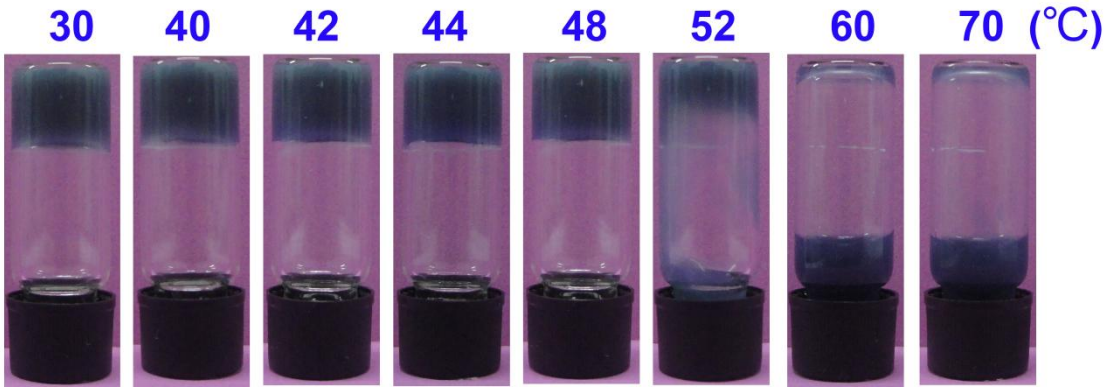

Figure S10. Digital photographs showing the thermo-responsive gel-sol transition of the as-prepared PNPG-PEG/*a*-CD hydrogel. The sol-gel transition temperature of hydrogel was determined by test-tube inverting method and estimated to be 52 ℃. The mixture was in gel phase below 52℃ and became flowable with increasing the temperature. The sol-gel transition was reversible upon the change of temperature. When the temperature was lowered, the hydrogel was gradually recovered from the sol phase. The character of thermo-sensitive and reversible gel-sol transition made this hydrogel suitable for locally controlled delivery of drugs.

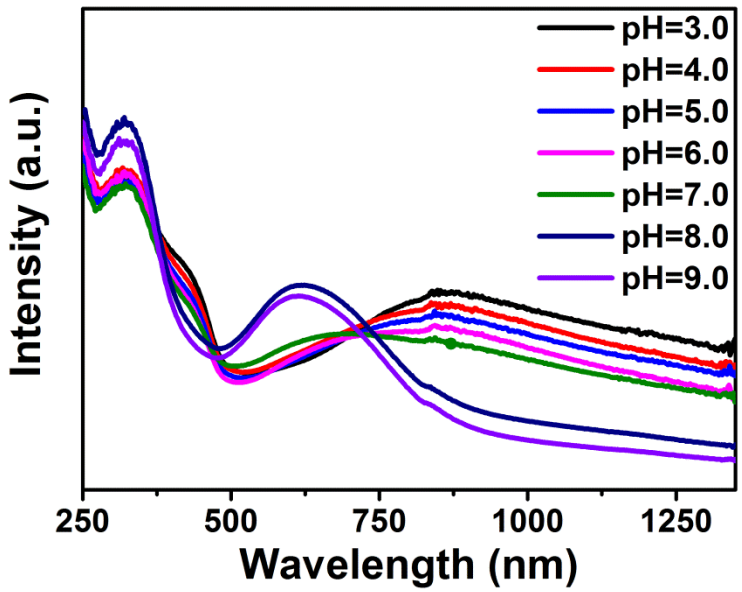

Figure S11. UV-vis-NIR absorbance spectra of PNPG-PEG in aqueous solutions with different pH values. In acid environments, the PNPG-PEG demonstrated broad and strong absorption that covered both NIR-I and NIR-II region (pH=3.0, 4.0, 5.0 and 6.0). Interestingly, the absorption intensity in NIR region was increased with the decrease of pH values. This absorption band was associated with the charge transfer between quinoid and benzenoid rings of PNPG. Nevertheless, this absorption band was blue-shifted back to the visible spectral region (630 nm) in alkaline environments (pH=8.0 and 9.0), which could be ascribed to the dedoping effect induced by change of pH values.[3, 12-14] These observations confirmed that the doping of PNPG was responsible for the strong and broad absorption that covered both NIR-I and NIR-II regions. Besides, the absorption peak located at 340 nm was related to the π–π* transition of the benzene rings. [6]

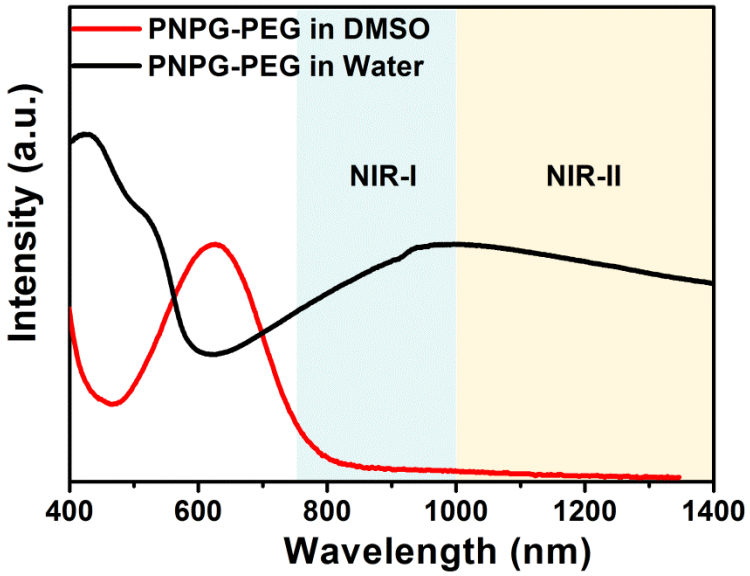

Figure S12. UV-vis-NIR absorbance spectra of PNPG-PEG in DMSO (aprotic solvent), and PNPG-PEG in water (protic solvent). In DMSO, an aprotic solvent, PNPG-PEG demonstrated negligible absorbance in the NIR spectral region, which was related to the dedoping effect. The absorption band associated with the charge transfer between quinoid and benzenoid rings of PNPG was centered at 632 nm, visible light region. For PNPG-PEG in water, this absorption band related to the charge transfer between quinoid and benzenoid rings of PNPG was red-shifted toward the NIR spectral region, resulting the broad and strong absorption that covered both NIR-I and NIR-II regions (from 750 nm to 1400 nm). This observation further confirmed that the doping of PNPG should be responsible for the strong and broad absorption that covered both NIR-I and NIR-II regions. That is, the doping effect redshifted the absorbance (associated with the charge transfer between quinoid and benzenoid rings) of PNPG from the visible light region to NIR spectral range. [3, 12-14]

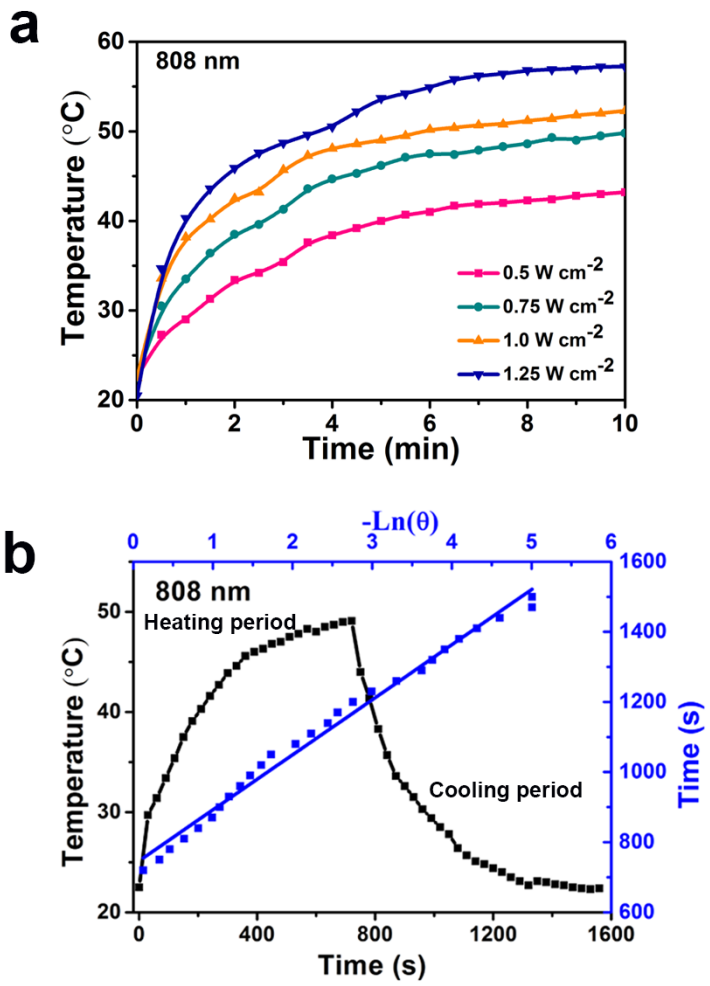

Figure S13. (a) Photothermal heating curves of PNPG-PEG dispersed aqueous suspensions (15 mg mL^{-1} in water) under 808 nm (NIR-I) laser irradiation at varied power densities; (b) Calculation of the photothermal conversion efficiency. Black line: photothermal heating curve of PNPG-PEG dispersed aqueous suspensions under the irradiation with 808 nm (NIR-I, laser power: 0.5 W cm^{-2}), and the cooling curve after the laser was switched off. Blue line: linear relationship between time of the cooling period and -lnθ, Time constant (τ) for the heat transfer from the system was determined by applying the linear time data from the cooling period and determined to be 158 s of 808 nm. The temperature increased with increasing power density and irradiation times. The photothermal conversion efficiency of PNPG-PEG composite was determined to be 40% under 808 nm laser irradiation.

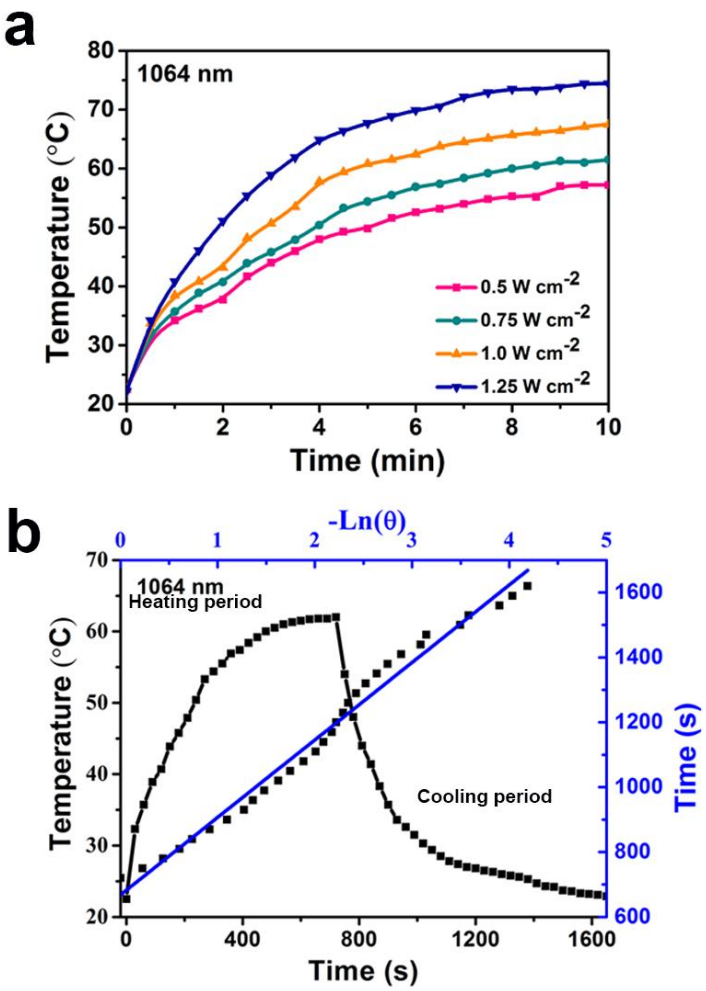

Figure S14. (a) Photothermal heating curves of PNPG-PEG dispersed aqueous suspensions (15 mg mL^{-1} in water) under 1064 nm (NIR-II) laser irradiation with at varied power densities; (b) Calculation of the photothermal conversion efficiency. Black line: photothermal heating curve of PNPG-PEG dispersed aqueous suspensions under the irradiation with 1064 nm (NIR-II, laser power: 0.5 W cm^{-2}), and the cooling curve after the laser was switched off. Blue line: linear relationship between time of the cooling period and -lnθ. Time constant (τ) for the heat transfer from the system was determined by applying the linear time data from the cooling period and determined to be 238 s of 1064 nm. The temperature increased with increasing power density and irradiation times. The photothermal conversion efficiency of PNPG-PEG composite was estimated to be 41% under 1064 nm laser irradiation.

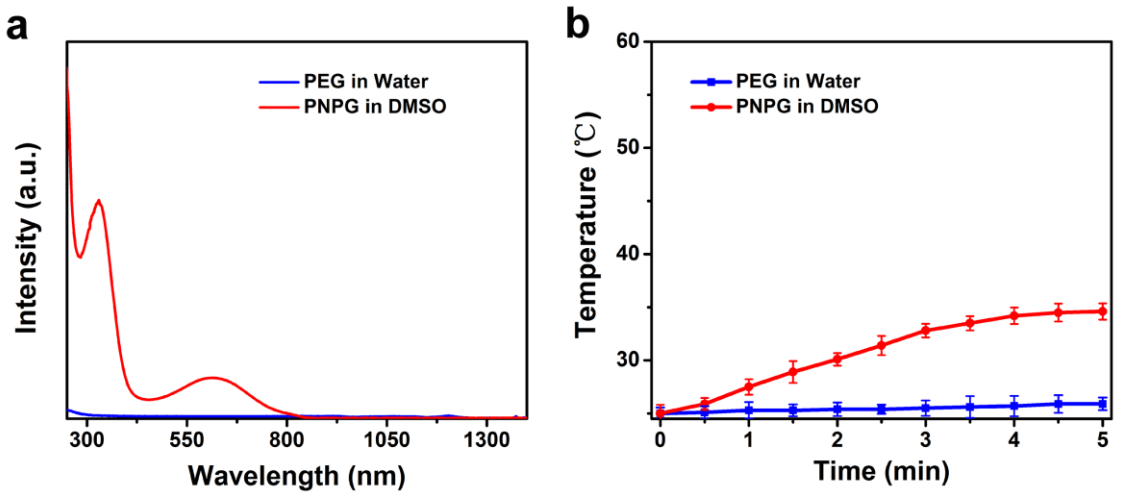

Figure S15. (a) UV-vis-NIR absorbance spectra of PEG in water and PNPG in DMSO; (b) Photothermal heating curves of PEG in water and PNPG in DMSO under 808 nm laser irradiation (0.5 W cm^{-2}, 5 minutes). It is obviously that the photothermal conversion efficiency of PEG was negligible, because of its negligible absorbance from visible light region to NIR spectral region. In the absence of PEG, the PNPG displayed poor dispersibility and formed precipitation in water (as shown in **figure S3**). Thus, we collected the UV-vis-NIR absorbance spectra and photothermal heating curves of PNPG in DMSO. PNPG in DMSO demonstrated negligible absorbance in the NIR spectral region, which was related to the dedoping effect. The absorption band associated with the charge transfer between quinoid and benzenoid rings of PNPG was centered at 619 nm, visible light region, similar as that of PNPG-PEG in DMSO (**figure S12**). Under the same laser irradiation condition (808 nm, 0.5 W cm^{-2}, 5 minutes), the temperature increment of the PNPG-PEG composite in water (19.6 ℃) was much higher than that of PNPG in DMSO (9.6 ℃). Moreover, considering that specific heat capacity of water is twice higher than that of DMSO, we can conclude that the photothermal conversion performance of PNPG-PEG is far superior to the PNPG (The specific heat capacity of DMSO and water is 1.95 kJ kg^{-1} K^{-1} and 4.20 kJ kg^{-1} K^{-1}, respectively).

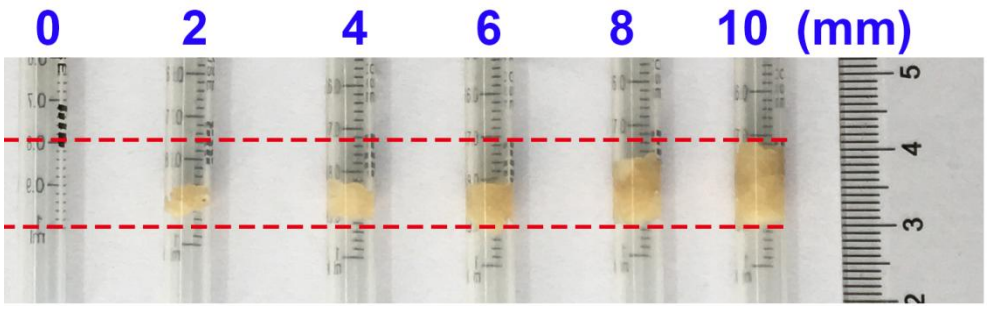

Figure S16. Different thicknesses (0, 2, 4, 6, 8, and 10 mm) of chicken breast tissues filled in transparent pipes were used as model biological tissues.

Figure S17. The thermo-sensitive and reversible gel-sol transition of the hydrogel under 1064 nm laser irradiation. Under NIR laser irradiation, localized photothermal effect induced by the hydrogel caused the thermo-responsive gel-sol transition of the hydrogel. When the laser irradiation was ceased, the hydrogel was gradually recovered from the sol phase. With the ability of undergoing reversible gel-sol transition under NIR laser irradiation, this supramolecular hydrogel could be capable of on-demand therapeutic drug release triggered by NIR laser.

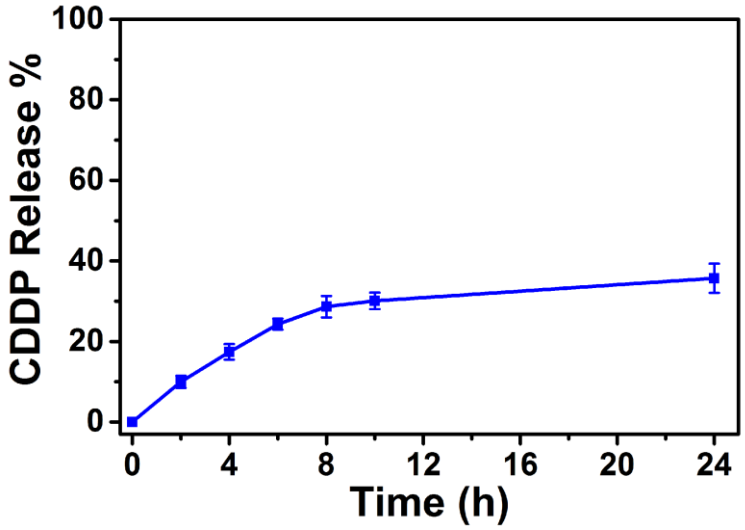

Figure S18. Long-term release of CDDP from the hydrogel without laser irradiation (in PBS solution; concentration of CDDP: 0.5 mg mL^{-1}). The initial burst release of CDDP (approximately 28%) at the initial 8 hours was probably related to the hydrophilic nature of CDDP.

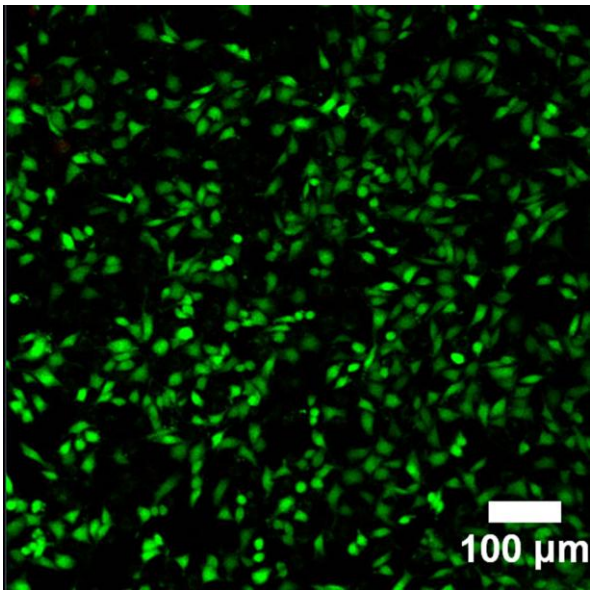

Figure S19. Confocal images of calcein AM (green, 488 nm excitation) and propidium iodide (PI, red, 543 nm excitation) co-stained L929 cells after incubation with PNPG-PEG/*a*-CD hydrogel (8 g L^{-1}, 48 hours). Almost all the cells were colored green without the presence of dead cells (red), confirming the good biocompatibility of this hydrogel.

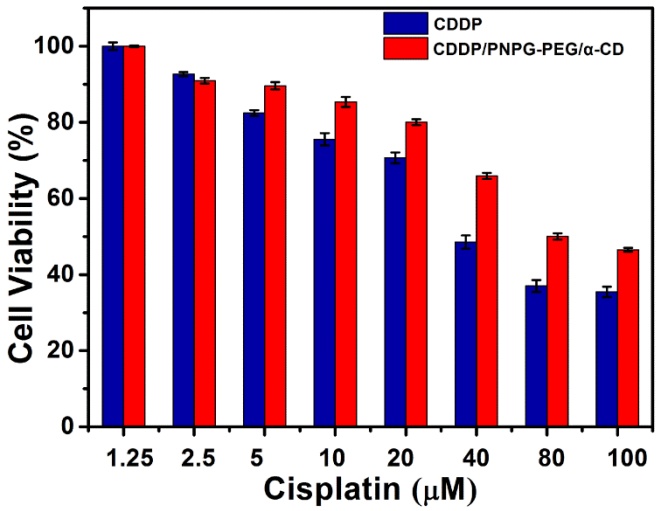

Figure S20. Viability of MDA-MB-231 cells after treatment with free CDDP (with varying concentrations) and CDDP/ PNPG-PEG/*α*-CD hydrogel (concentration of hydrogel: 8 g L^{-1}; without laser irradiation) for 48 h (n=6). The amount of CDDP in the CDDP/PNPG-PEG/*α*-CD hydrogel was same as that of free CDDP group. The standard MTT assay was used to assess the cell viability.

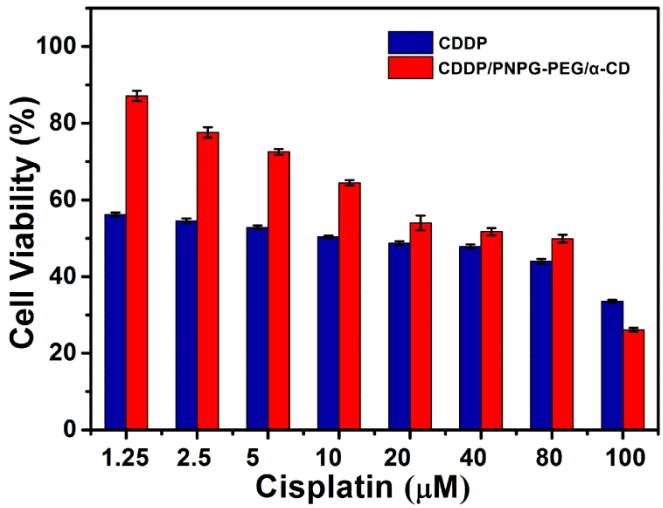

Figure S21. Viability of MCF-7 cell after treatment with free CDDP (with varying concentrations) and CDDP/ PNPG-PEG/*α*-CD hydrogel (concentration of hydrogel: 8 g L^{-1}; without laser irradiation) for 48 h (n=6). The amount of CDDP in the CDDP/PNPG-PEG/*α*-CD hydrogel was same as that of free CDDP group. The standard MTT assay was used to assess the cell viability.

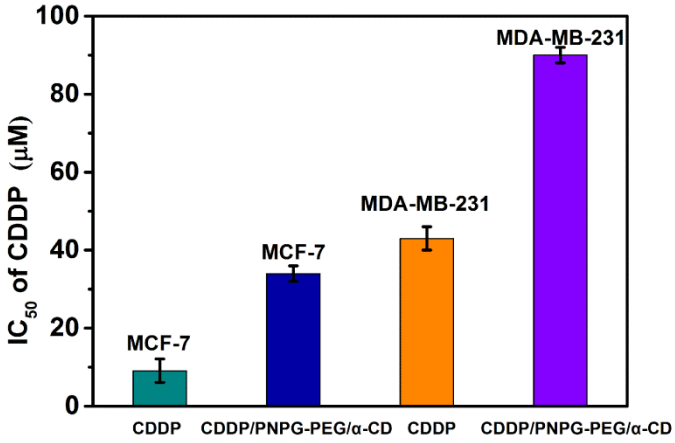

Figure S22. The half maximal inhibitory concentrations (IC_{50} values) of free CDDP and CDDP loaded in CDDP/PNPG-PEG/α-CD hydrogel (without laser irradiation) after 48 hours of treatment. MDA-MB-231 cells and MCF-7 cell are both human breast cancer cell lines. MCF-7 cells express estrogen receptor, progesterone receptor, but not the Her2/Neu receptor. This cell line is often responsive to chemotherapy. MDA-MB-231 cells are triple negative breast cancer (TNBC) cell line, lacking all three receptors, and thus are highly aggressive, and often resistant to chemotherapy.[15-17] The viability studies on MCF-7 cells were performed as control group to confirm that MDA-MB-231 cell model was cisplatin resistant. The high IC_{50} value of free CDDP towards MDA-MB-231 cells indicated that MDA-MB-231 cancer cell model was cisplatin resistant. The higher IC_{50} values of CDDP in CDDP/ PNPG-PEG/α-CD hydrogel than that of free CDDP was ascribed to the slow and sustained release of CDDP from the CDDP/ PNPG-PEG/α-CD hydrogel.

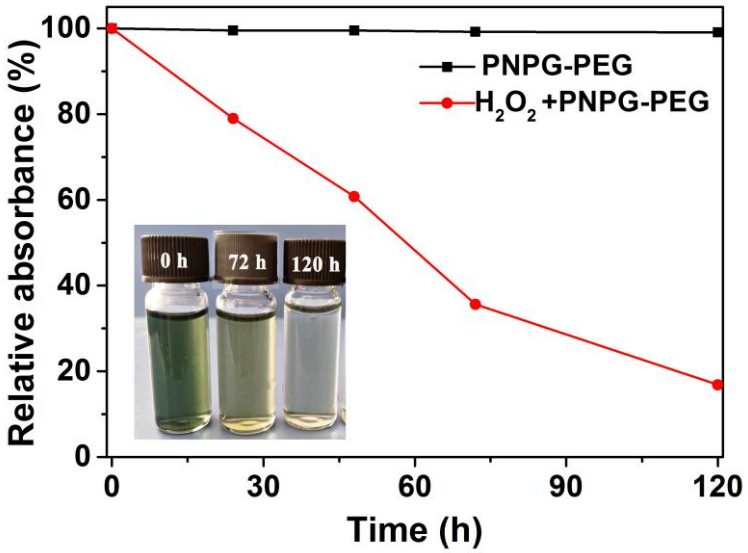

Figure S23. The degradation of PNPG-PEG composite in hydrogen peroxide. We monitored the degradation of PNPG-PEG composite in hydrogen peroxide using UV-vis-NIR spectroscopy. The absorbance intensity of PNPG-PEG at 1064 nm was gradually reduced coupled with color fading in the presence of hydrogen peroxide. Hydrogen peroxide is an endogenous molecule produced by reduced nicotinamide adenine dinucleotide phosphate (NADPH) oxidases, which widely exists in phagocytes and many organs. This observation suggested that PNPG-PEG composite was probably degraded by the oxidative environment *in vivo*.[18]

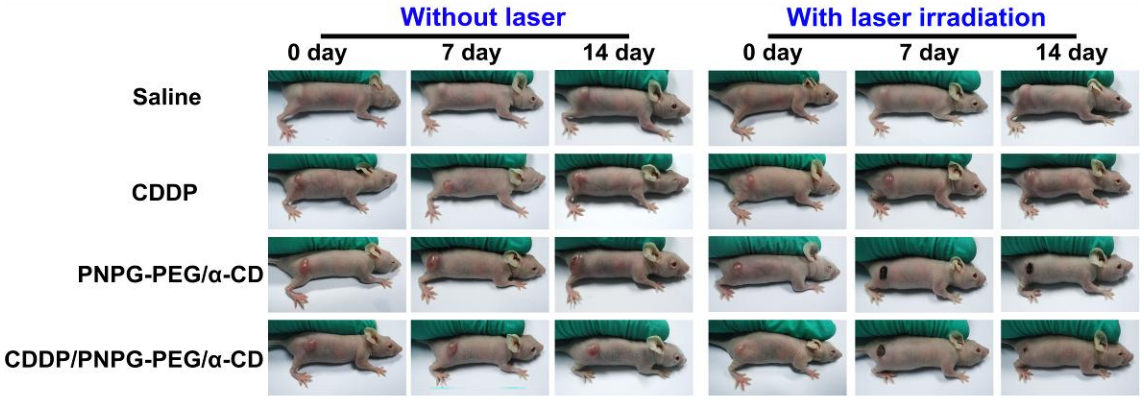

Figure S24. Digital photos of triple-negative breast cancer (TNBC)-bearing mice during different administrations. Animals bearing implanted tumors were treated with intratumoral injection of: (1, 2) 100 μL of saline; (3, 4) 100 μL of free CDDP solution by multiple injections (at total doses of 8 mg CDDP/kg body weight; injection of 2 mg CDDP/kg body weight at day 0, 2, 4, 6, respectively); (5, 6) 100 μL of PNPG-PEG/*a*-CD hydrogel ((*via* a single injection); and (7, 8) 100 μL of CDDP/PNPG-PEG/*a*-CD hydrogel (*via* a single injection, at doses of 8 mg CDDP/kg body weight), respectively. 4 hours after the injections, the groups labeled with 2, 4, 6, and 8 were treated with the first cycle of 1064 nm laser irradiation (5 minutes; power density: 0.5 W cm^{-2}) at the tumor sites. During the period of administrations, groups 2, 4, 6, and 8 were treated with a total of four cycles of 1064 nm laser irradiation (at 0, 2, 4 and 6 days following injections, 5 minutes each cycle; under a low power density of 0.5 W cm^{-2}).

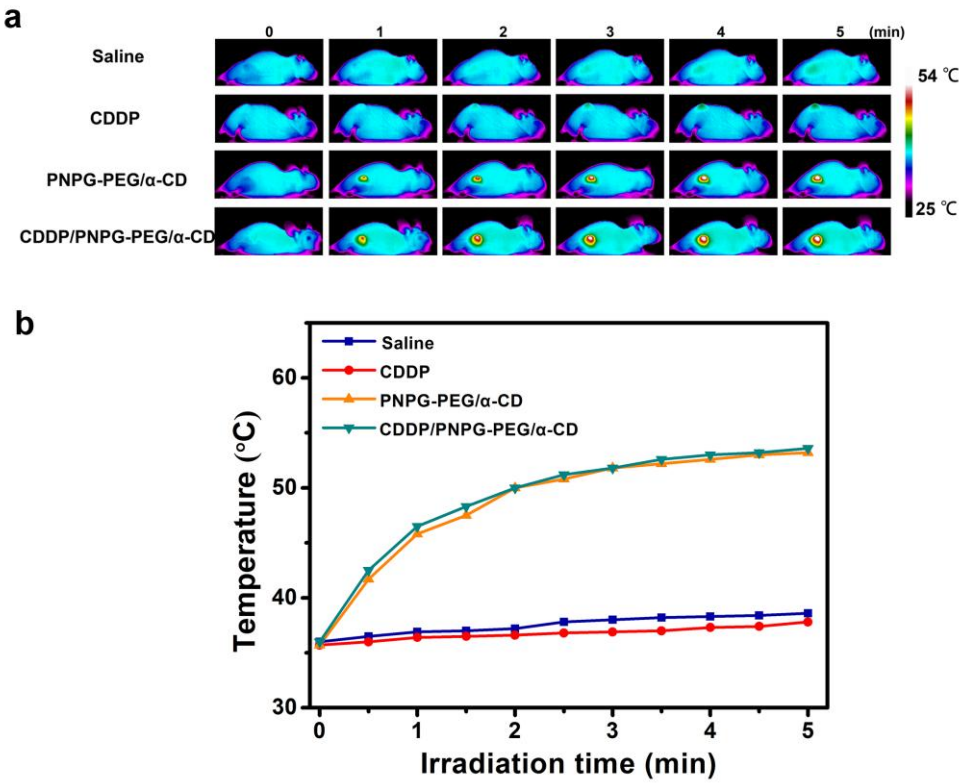

Figure S25. (a) Infrared thermal images of MDA-MB-231 tumor-bearing mice after injection of single dose of saline, free CDDP, PNPG-PEG/*α*-CD hydrogel and CDDP/ PNPG-PEG/*α*-CD hydrogel, followed by exposure to 1064 nm NIR laser (laser power: 0.5 W cm^{-2}; irradiation time: 5 minutes); (b) The corresponding tumor temperature change profiles of the irradiated area. It is obvious that the loading of CDDP into the hydrogel had no adverse effect on the temperature elevation.

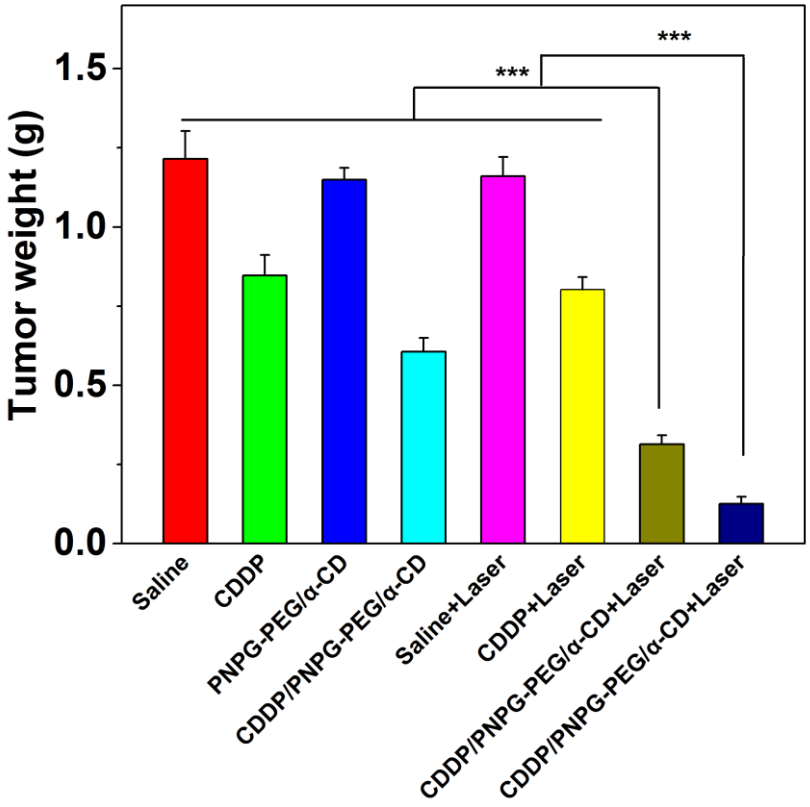

Figure S26. Tumor weight of all the tumors excised at the end of treatments (2 weeks after the injection). Data are presented as a mean ± SD (n=3, Significance is defined as $^{***}P < 0.001$.)

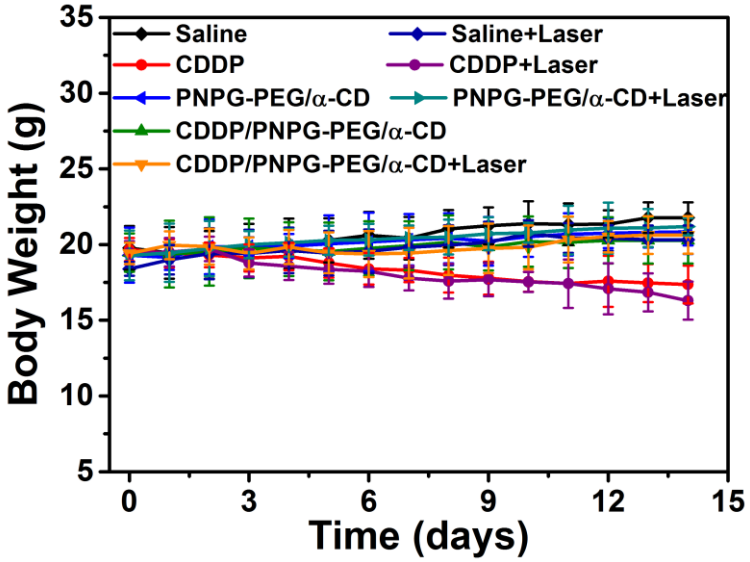

Figure S27. Time-dependent body weight curves of the triple-negative breast cancer (TNBC)-bearing mice during different administrations. No apparent body weight loss was observed during the therapeutic period for the groups treated with CDDP/PNPG-PEG/*a*-CD hydrogel (with and without laser), indicating reduced side effects related to the toxicity of CDDP. In contrast, treatment with free CDDP led to obvious loss of body weight, implying the side effects caused by the toxicity of CDDP. The other four control groups (treated with saline, saline plus laser, PNPG-PEG/*a*-CD hydrogel alone, and PNPG-PEG/*a*-CD hydrogel plus laser) also showed steady body weight increases.

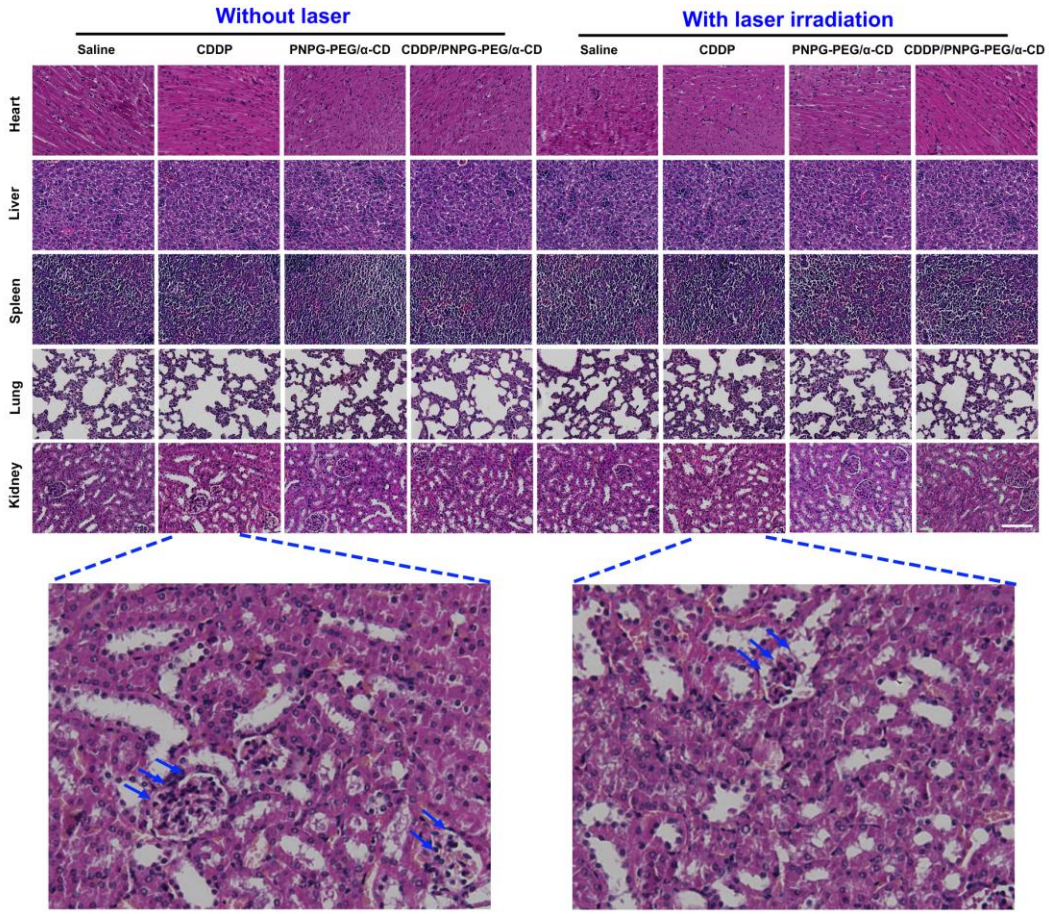

Figure S28. H&E staining of the organs tissues (including heart, liver, spleen, lung and kidney) after the treatments (Scale bar: 100 μm). In the (H&E) staining, the nuclei were stained bluish violet, and the cytoplasm and extracellular matrix were stained pink. For the four groups treated with PNPG-PEG/*a*-CD hydrogel and CDDP/PNPG-PEG/*a*-CD hydrogel (with or without laser irradiation), the H&E staining of the major organs tissues (including heart, liver, spleen, lung and kidney) showed no obvious pathological changes compared to these from the groups treated with saline. No detectable lesions, such as necrosis, hydropic degeneration, inflmmatory, pulmonary firosis, were observed in the sections of these tissues, indicating that the PNPG-PEG/*a*-CD hydrogel was biocompatible and the toxicity of CDDP was reduced by encapsulating CDDP into this hydrogel.[19-23] For the groups treated with free CDDP (with or without laser irradiation), kidney tissues dispalyed the obvious disappearance of renal capsule cavity (marked by arrows), indicating the nephrotoxicity caused by free CDDP. [21-23]

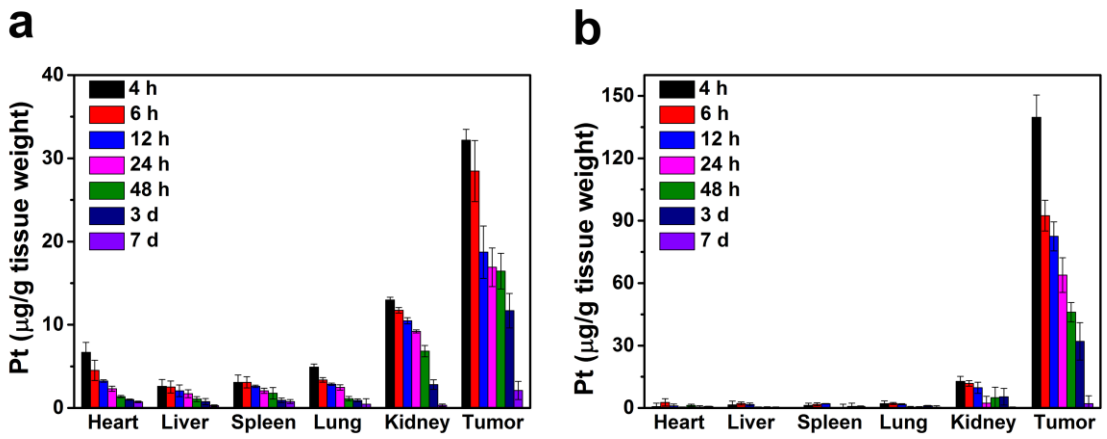

Figure S29. The biodistribution of CDDP in the tumors and the major organs (including heart, liver, spleen, lung and kidney) after the intratumoral injection of (a) free CDDP (*via* a single injection, at doses of 4 mg CDDP/kg body weight) and (b) CDDP/PNPG-PEG/*a*-CD hydrogel (100 μL, *via* a single injection, at doses of 4 mg CDDP/kg body weight). At different time points (4 hours, 6 hours, 12 hours, 24 hours, 48 hours, 3 days and 7 days) after the injection, the mice were sacrificed and the distribution of Pt in tumors and major organs (heart, liver, spleen, lung and kidney) was monitored by ICP-MS analysis. These organs were lyophilized and weighed before digestion in aqua regia for 2 h at 80℃ for dissolution of the tissues. Thereafter, concentrations of Pt were quantified by ICP-MS. Clearly, for the group injected with CDDP/PNPG-PEG/*a*-CD hydrogel, the CDDP mainly concentrated at the tumor sites, with less nonspecific distribution to the major organs. This observation confirmed that the PNPG-PEG/*a*-CD hydrogel could effectively maintain higher accumulation rate of the CDDP in tumors, as compared with the free CDDP groups.

Table S1. Photothermal performance of recently reported photothermal agents (mainly conjugated polymers and some inorganic nanoparticles in NIR II window).

photothermal agents	*C*	laser	laser power (W/cm^2)	irradiation time (minutes)	ΔT (℃)	η (%)	References
PNPG-PEG	15 mg/ml	808 nm 1064 nm	0.5	5	25.2 26.4	40 41	this work
Ultrathin PPy Nanosheets	100 μg/ml	808 nm 1064 nm	1	5	34.6 40.2	55.6 64.6	*Nano Letters*, 2018, **18**, 2217-2225.
thieno-isoindigo derivative-based polymer: PBTPBF-BT	30.0 μg/mL	1064 nm	2	5	31.4	66.4	*Biomaterials*, 2018, 155 103-111.
polyaniline nanoparticles: PANPs	1 mg/mL	808 nm	0.5	5	24.4	48.5	*Biomaterials*, 2013, **34**, 9584-9592.
thiophene-derived π-conjugated polymer: TBDOPV-DT	0.88 mg/mL	1064 nm	1.3	10	19.4	49.2	*Chem. Mater.*, 2017, **29**, 718-725.
polyaniline nanoparticles: PANPs	0.5 mg/mL	808 nm	2.45	3	38	-	*Angew. Chem. Int. Ed.*, 2011, **50**, 441-444.
$(NH_4)xWO_3$ nanocube	2 mg/ml	1064 nm	1.4	10	48	39.4	*Biomaterials*, 2015, **52**, 407-416.
Cu_9S_5 nanocrystals	40 ppm	980 nm	0.51	7	15.1	25.7	*ACS Nano*, 2011, **5**, 9761-9771.
black hollow silicon oxide nanoparticles: H-SiOx-PEG NPs	36 ppm	1064 nm	1	25	23	48.6	*Biomaterials*, 2017, **143**, 120-129.

References

[1] P. Lei, R. An, P. Zhang, S. Yao, S. Song, L. Dong, X. Xu, K. Du, J. Feng and H. Zhang, *Adv. Funct. Mater.* 2017, **27**, 1702018.

[2] D. K. Roper, W. Ahn and M. Hoepfner, *J. Phys. Chem. C*, 2007, **111**, 3636-3641.

[3] B.-P. Jiang, L. Zhang, Y. Zhu, X.-C. Shen, S.-C. Ji, X.-Y. Tan, L. Cheng and H. Liang, *J. Mater. Chem. B*, 2015, **3**, 3767-3776.

[4] Y. Duan, Q. Tang, Y. Chen, Z. Zhao, Y. Lv, M. Hou, P. Yang, B. He and L. Yu, *J. Mater. Chem. A*, 2015, **3**, 5368-5374.

[5] H. Xu, J. Liu, Y. Chen, J. Tang and Z. Zhao, *J. Appl. Polym. Sci.*, 2016, DOI: 10.1002/APP.44248.

[6] C. Li, N. Chartuprayoon, W. Bosze, K. Low, K. H. Lee, J. Nam and N. V. Myung, *Electroanalysis*, 2014, **26**, 711-722.

[7] Q. Lin, Y. Yang, Q. Hu, Z. Guo, T. Liu, J. Xu, J. Wu, T. B. Kirk, D. Ma and W. Xue, *Acta Biomater*, 2017, **49**, 456-471.

[8] J. Yu, W. Ha, J. N. Sun and Y. P. Shi, *ACS Appl. Mater. Interfaces*, **2014**, *6*, 19544-19551.

[9] G. D'Errico, M. De Lellis, G. Mangiapia, A. Tedeschi, O. Ortona, S. Fusco, A.

Borzacchiello and L. Ambrosio, *Biomacromolecules* 2008, **9**, 231-240.

[10] C. Wang, X. Wang, K. Dong, J. Luo, Q. Zhang and Y. Cheng, *Biomaterials*, 2016, **104**, 129-137.

[11] X. Wang, C. Wang, Q. Zhang and Y. Cheng, *Chem. Commun.*, 2016, **52**, 978-981.

[12] J. Yang, J. Choi, D. Bang, E. Kim, E.-K. Lim, H. Park, J.-S. Suh, K. Lee, K.-H. Yoo, E.-K. Kim, Y.-M. Huh and S. Haam, *Angew. Chem. Int. Ed.*, 2011, **50**, 441-444.

[13] B.-P. Jiang, L. Zhang, X.-L. Guo, X.-C. Shen, Y. Wang, Y. Zhu and H. Liang, *Small*, 2017, **13**, 1602496.

[14] C. W. Hsiao, E. Y. Chuang, H. L. Chen, D. Wan, C. Korupalli, Z. X. Liao, Y. L. Chiu, W. T. Chia, K. J. Lin and H. W. Sung, *Biomaterials*, 2015, **56**, 26-35.

[15] C. J. Bowerman, J. D. Byrne, K. S. Chu, A. N. Schorzman, A. W. Keeler, C. A. Sherwood, J. L. Perry, J. C. Luft, D. B. Darr, A. M. Deal, M. E. Napier, W. C. Zamboni, N. E. Sharpless, C. M. Perou and J. M. DeSimone, *Nano Lett.*, 2017, **17**, 242-248.

[16] Q. Ni, Z. Teng, M. Dang, Y. Tian, Y. Zhang, P. Huang, X. Su, N. Lu, Z. Yang, W. Tian, S. Wang, W. Liu, Y. Tang, G. Lu and L. Zhang, *Nanoscale* 2017, **9**, 1466-1474.

[17] F. Zhou, B. Feng, T. Wang, D. Wang, Z. Cui, S. Wang, C. Ding, Z. Zhang, J. Liu, H. Yu and Y. Li, *Adv. Funct. Mater.*, 2017, **27**, 1703674.

[18] Y. Liu, K. Ai, J. Liu, M. Deng, Y. He and L. Lu, *Adv. Mater.*, 2013, **25**, 1353-1359.

[19] W. Guo, C. Guo, N. Zheng, T. Sun and S. Liu, *Adv. Mater.*, 2017, **29**, 1604157.

[20] H. Lin, S. Gao, C. Dai, Y. Chen and J. Shi, *J. Am. Chem. Soc.*, 2017, **139**, 16235-16247.

[21] S. Yu, D. Zhang, C. He, W. Sun, R. Cao, S. Cui, M. Deng, Z. Gu and X. Chen, *Biomacromolecules*, 2017, **18**, 4341-4348.

[22] S. Li, C. Li, S. Jin, J. Liu, X. Xue, A. S. Eltahan, J. Sun, J. Tan, J. Dong and X. J. Liang, *Biomaterials*, 2017, **144**, 119-129.

[23] X. Wu, Y. Wu, H. Ye, S. Yu, C. He and X. Chen, *J. Control. Release*, 2017, **255**, 81-93.